Kinetic simulation of secondary electron emission effects in Hall thrusters

D. Sydorenko[a)] and A. Smolyakov
*Department of Physics and Engineering Physics, University of Saskatchewan, Saskatoon,
Saskatchewan S7N 5E2, Canada*

I. Kaganovich and Y. Raitses
Princeton Plasma Physics Laboratory, Princeton University, Princeton, New Jersey 08543

The particle-in-cell code has been developed for kinetic simulations of Hall thrusters with a focus on plasma-wall interaction. It is shown that the effect of secondary electron emission on wall losses is different from predictions of previous fluid and kinetic studies. In simulations, the electron velocity distribution function is strongly anisotropic, depleted at high energy, and nonmonotonic. Secondary electrons form two beams propagating between the walls of a thruster channel in opposite radial directions. The beams produce secondary electron emission themselves depending on their energy at the moment of impact with the wall, which is defined by the electric and magnetic fields in the thruster as well as by the electron transit time between the walls. The condition for the space-charge-limited secondary electron emission depends not only on the energy of bulk plasma electrons but also on the energy of beam electrons. The contribution of the beams to the particles and energy wall losses may be much larger than that of the plasma bulk electrons. Recent experimental studies may indirectly support the results of these simulations, in particular, with respect to the electron temperature saturation and the channel width effect on the thruster discharge. © *2006 American Institute of Physics*. [DOI: 10.1063/1.2158698]

Operation of a Hall thruster is strongly affected by the secondary electron emission (SEE) from thruster channel walls. SEE decreases the plasma potential and thus increases the flux of electrons from plasma to the wall.[1] With the growth of plasma electron temperature the emission coefficient γ increases until at some critical electron temperature T_{cr} it reaches the critical value γ_{cr} and the SEE turns to the space-charge-limited (SCL) regime. Here $\gamma = \Gamma_2/\Gamma_1$, Γ_1 and Γ_2 are the primary and the secondary electron fluxes, $\gamma_{cr} \simeq 1 - 8.3(m/M)^{1/2}$, and m and M are the electron and the ion mass. In the SCL regime part of emitted electrons is reflected by the negative potential drop near the wall. Transition to the SCL regime is accompanied by the considerable growth of the primary electron flux and is an important factor limiting the electron temperature. For boron nitride ceramics grade HP, which is used in some Hall thrusters, the critical electron temperature of a plasma with a Maxwellian electron velocity distribution function (EVDF) is $T_{cr} = 18.26$ eV.[2] The fluid theories describing Hall thrusters[3–6] assume that the EVDF is Maxwellian and predict fast electron cooling due to wall losses and saturation of the electron temperature with the growth of the discharge voltage. In fact, such saturation was recently measured in a 2 kW Hall thruster;[7] however, the electron temperature inside the thruster channel was several times higher than T_{cr}.[7,8] Kinetic studies of plasmas in Hall thrusters[9,10] reveal the depletion of the high-energy tail of EVDF and the reduction of the electron losses to the wall compared with fluid theories. It was shown in Ref. 11 for electron cyclotron resonance discharges that EVDF near a wall is non-Maxwellian and strongly anisotropic. Thus, the

proper analysis of EVDF in Hall thrusters requires kinetic plasma simulations.

In the accelerating region of a Hall thruster the radial magnetic field is strong and the EVDF is established on a spatial scale much smaller than the accelerating region length. Therefore, to obtain the EVFD it is sufficient to consider a thin radial section of the accelerating region, which may be approximated by a one-dimensional model. Consider a plasma bounded by two infinite parallel dielectric walls with SEE, see Fig. 1. Axis x is directed normal to the walls. The system is uniform along axes y and z. The plasma is immersed in the external constant uniform magnetic field B_x and electric field E_z. The described system is simulated with the parallel electrostatic particle-in-cell code[12,13] developed on the basis of the direct implicit algorithm.[14,15] The code resolves one spatial coordinate x and three velocity components v_x, v_y, and v_z for each particle. Elastic, excitation, and ionization collisions between electrons and neutral xenon atoms are implemented, making use of the Monte Carlo model of collisions.[16] The uniform neutral gas density is constant during simulations. To account for the anomalously high electron mobility across the magnetic field in Hall thrusters, the additional "turbulent" collisions are introduced,[4,17] which randomly scatter particles in y-z plane without changing their energy.[18] Coulomb and ion-neutral collisions are neglected.[17] The SEE model is similar to that of Ref. 19. The total emission coefficient γ agrees with the available experimental data for boron nitride ceramics grade HP.[20] The ions are neutralized after collision with the wall increasing the surface charge.

Parameters of simulations correspond to the values experimentally measured in the 2 kW Hall thruster for dis-
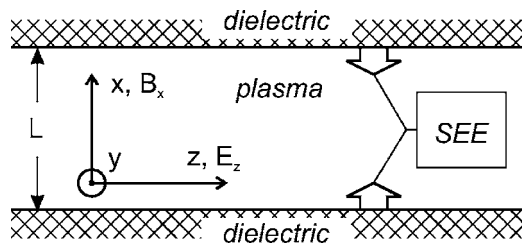
a)Electronic mail: dms169@mail.usask.ca

13, 014501-1

FIG. 1. Schematic diagram of the simulated plasma system. The two dielectric walls represent the coaxial ceramic channel of a Hall thruster.

FIG. 2. EVDF over v_x and v_z in the middle of the plasma 10 mm$<x$ <15 mm plotted in energy coordinates (the sign marks the velocity direction). (a) 3D plot; (b) the corresponding 2D plot with contour lines. Any two neighbor contour lines in (b) have a level difference of 0.1. The plasma potential relative to the wall is $\Phi=20$ V.

charge voltages from 200 to 350 V.[21] The axial electric field E_z and the radial magnetic field B_x are taken at the point with maximal electron temperature, which is inside the thruster channel for the considered discharge voltage range. The neutral gas density n_a determines the frequency of electron-neutral collisions ν_{en}. The turbulent collision frequency ν_t is adjusted such that the electron mobility μ_c due to both turbulent and electron-neutral collisions corresponds to the experimental value of the electron electric current density J_{exp},

$$J_{\text{exp}} = en_e\mu_c E_z = en_e \frac{e(\nu_t + \nu_{\text{en}})}{m[(\nu_t + \nu_{\text{en}})^2 + \omega_c^2]} E_z,$$

where $-e$ is the electron charge, n_e is the electron density, and ω_c is the electron cyclotron frequency. Below the major results are highlighted, presenting for illustrations the simulation data corresponding to the discharge voltage of 350 V. In this simulation $L=2.5$ cm, $E_z=200$ V/cm, $B_x=100$ G, n_a $=2\times10^{12}$ cm^{-3}, and $\nu_t=1.46\times10^6$ s^{-1}; the plasma density averaged over the width of the plasma slab is $\langle n_e\rangle=3.2$ $\times10^{11}$ cm^{-3} after 6.9 μs of the system evolution.

The simulations reveal that in thruster plasmas the EVDF is anisotropic and far from Maxwellian (see Fig. 2).[13,22] The average energy of electron motion in the directions parallel to the walls $\langle w_{y,z}\rangle=\langle m v_{y,z}^2/2\rangle$ is several times larger than the average energy of electron motion in the direction perpendicular to the walls $\langle w_x\rangle=\langle m v_x^2/2\rangle$. The EVDF presented in Fig. 2 has $\langle w_x\rangle\simeq5.7$ eV and $\langle w_z\rangle\simeq24.5$ eV.

Qualitatively, the anisotropy of the EVDF can be explained as follows.[13,22] The electrons gain their energy from the accelerating electric field E_z as a result of turbulent collisions and collisions with neutral atoms. After a collision occurs the guiding center of electron's orbit displaces along z and the electron energy increases by $\Delta w\simeq eE_z r_L$, where r_L is the electron's Larmor radius. This energy increment Δw is distributed between w_y and w_z due to cyclotron rotation; thus, the heating occurs in the direction parallel to the walls. In addition, the electron-neutral collisions may turn the electron towards the wall. Electrons with $w_x>e\Phi$, where Φ is the plasma potential relative to the wall, form the loss cone, and quickly leave the plasma. Electrons with total kinetic energy $w=m(v_x^2+v_y^2+v_z^2)/2$ below the confinement threshold $e\Phi$ have to be heated before they can be scattered to the loss cone by electron-neutral collisions.[11,13] The electron-neutral collisions tend to make the EVDF isotropic in the energy region $w<e\Phi$. However, if $\nu_t\gg\nu_{\text{en}}$ the electrons gain energy in the directions parallel to the walls much faster than this energy is transferred via electron-neutral collisions to the
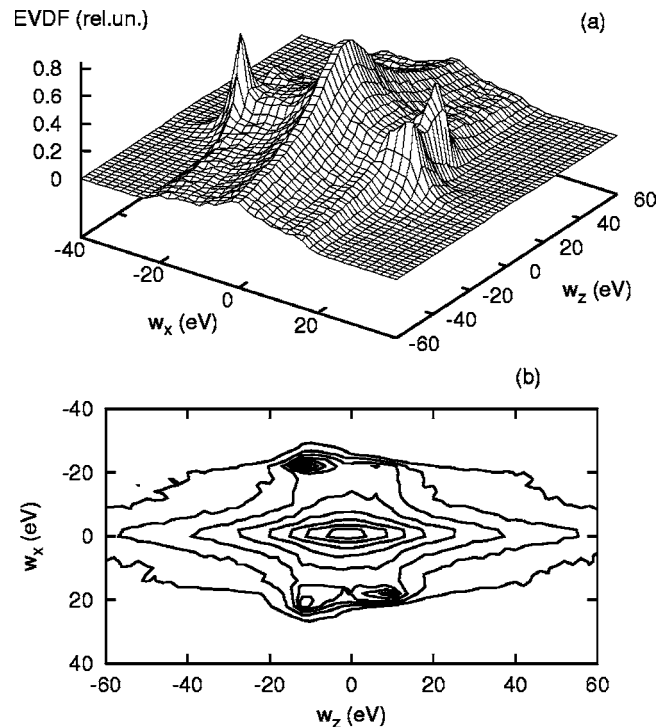
motion normal to the walls, resulting in the anisotropic EVDF.[11,22] The dominating anomalous conductivity is typical for simulations of the low discharge voltage regimes of 200–300 V. In simulation of the higher discharge voltage regime of 350 V the difference between the classical and the anomalous axial electron mobility decreases so that $\nu_t\sim\nu_{\text{en}}$. Here the anisotropy develops because the axial electric field E_z is so strong that after a collision the increment of the energy of motion parallel to the walls is $\Delta w>e\Phi$. As a result the subsequent electron-neutral collision may scatter this electron to the loss cone and the isotropization does not occur. Note that the low-energy electrons are permanently replenished due to ionization.

Although the SEE decreases the drop of potential across the sheath, the potential of plasmas with an isotropic Maxwellian EVDF remains above the electron temperature even in the SCL regime. In the present simulations the plasma potential, on the one hand, exceeds average energy of electron motion normal to the walls (compare curves 3 and 2 in Fig. 3). On the other hand, the plasma potential is small compared to the average energies of electron motion in the directions parallel to the walls $e\Phi<\langle w_{y,z}\rangle$ (compare curves 3 and 1 in Fig. 3). Thus, for a given average electron energy the electrostatic potential of the plasma with the anisotropic EVDF is far less than that of the plasma with the isotropic Maxwellian EVDF. Also, in the present simulations the electric field and the dynamics of plasma particles are calculated self-consistently across the whole plasma slab. As a result, the source sheaths, which are inherent in simulations with a
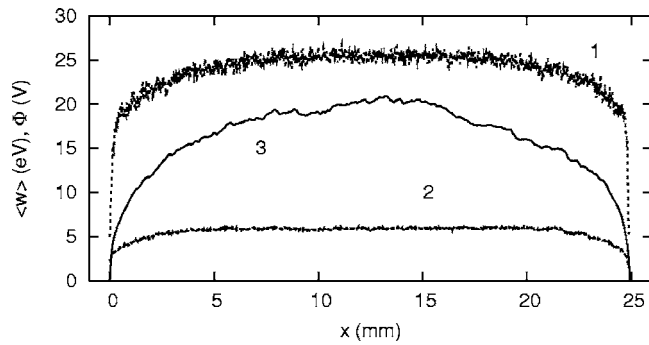
FIG. 3. Spatial profiles of the average electron energy of motion in z direction (curve 1) and in x direction (curve 2), and of the electrostatic potential (curve 3). The walls are at $x=0$ and $x=25$ mm. Note that everywhere $\langle w_x \rangle < e\Phi < \langle w_z \rangle$.

FIG. 4. For the electron beam emitted from the wall $x=0$: (a) represents the local flow velocities u_y (black triangles) and u_z (open triangles) vs x coordinate and (b) represents the local average energy $w_y + w_z$ vs x coordinate. The walls are at $x=0$ and $x=25$ mm.

plasma source and represent the distinct potential drop near the plasma source,[23,24] do not appear and the potential profile is smooth (curve 3 in Fig. 3).

For the neutral density used in simulations the average frequency of electron-neutral collisions is $\nu_{en} \simeq 1.4 \times 10^6$ s^{-1}, the mean free path in x direction between the two collisions with neutral atoms (which may scatter an electron towards the wall) is $\lambda_c \simeq 1$ m. The mean free path is much larger than the width of the plasma slab $\lambda_c \gg L$, that is why the EVDF is strongly depleted for the energies w_x above the plasma potential $w_x > e\Phi(x)$, i.e., in the loss cone.[11] The loss cone is populated by the electrons from the plasma bulk collided with neutral atoms, as well as by the electrons emitted from the bounding walls and accelerated in opposite directions by the sheath potential.

The emitted electrons form two counterpropagating electron beams. The electrons of these beams move along the spiral-like trajectories: the acceleration and deceleration in x direction (between the channel walls) are combined with the cyclotron rotation in y-z plane and $E_z \times B_x$ drift in y direction [see Fig. 4(a)]. The near-wall conductivity (NWC) theory relies on such motion explaining the increase of the electron mobility across the magnetic field.[25] In the simulation presented here the 200% increase of the axial electron mobility due to NWC compared to the mobility determined by collisions with neutral atoms and turbulent collisions is observed.[13,22] When NWC is significant, the profile of the axial electron current density $J_z(x)$ becomes modulated, as it is predicted in Ref. 25; see Fig. 5.

The energy of motion of emitted electron parallel to the walls also oscillates along the electron trajectories [see Fig. 4(b)]. At the time of collision with the wall the average energy of beam electrons w_b exceeds the initial average energy of emission by the value of the order of $m(E_z/B_x)^2$ due to the drift motion. Therefore, in large electric field the emitted electrons may produce intense secondary electron emission themselves.[13,22] From Fig. 4(b) it follows that w_b depends on the phase of cyclotron rotation of electrons at the moment of their impact with the wall. This phase depends on the time of transit of the emitted electrons between the walls and is defined by the distance between the walls and by the potential profile. Recently the strong effect of the channel width on
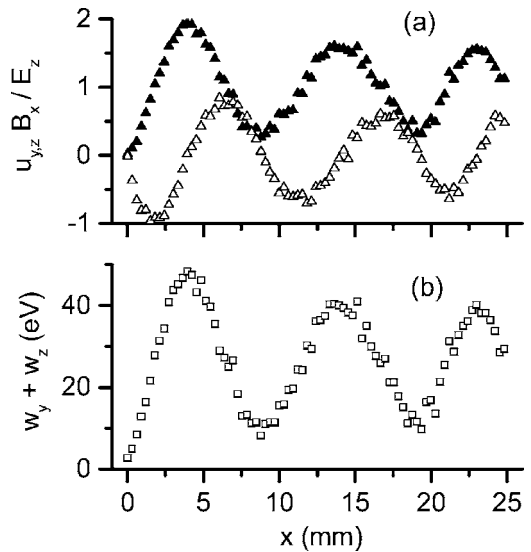
thruster operation has been observed,[21] which may be related with the dependence of the energy of the secondary electron beams on the width of the channel.

The plasma bulk electrons and the beam electrons are characterized by different average energies w_p and w_b at the moment of impact with the wall, and thus produce SEE with independent partial emission coefficients γ_p and γ_b. Here, subscripts p and b correspond to the plasma bulk and the beam electrons. Consider the stationary state of the system with symmetric monotonic potential profiles near the walls. For each dielectric wall the ratio of the fluxes of electrons of the bulk plasma and of the secondary electron beam towards one of the walls is[13,22]

$$\frac{\Gamma_b}{\Gamma_p} = \frac{\alpha \gamma_p}{1 - \alpha \gamma_b}, \qquad (1)$$

where Γ_p is the primary electron flux due to the bulk plasma electrons, Γ_b is the primary electron flux due to the beam of electrons emitted from the opposite wall, $\alpha = \Gamma_b/\Gamma_2 < 1$ is the coefficient of penetration of the electron beam through the plasma slab, and Γ_2 is the total secondary electron flux emit-
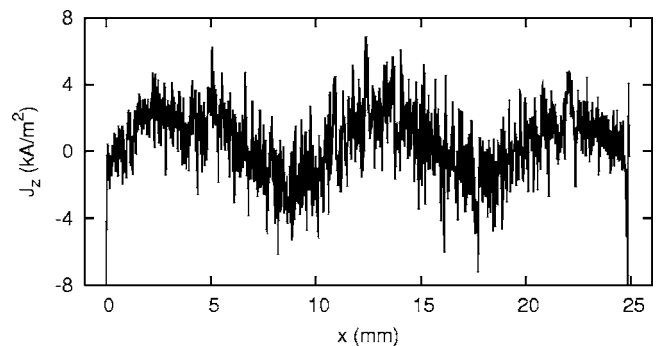

FIG. 5. Modification of the profile of the electron current density in z direction due to NWC. The walls are at $x=0$ and at $x=25$ mm.

ted by that opposite wall. Equation (1) is valid if $\alpha\gamma_b < 1$—otherwise the stationary stage is not possible. From (1) it follows that if $\alpha\gamma_p \gg 1 - \alpha\gamma_b$ then $\Gamma_b \gg \Gamma_p$ and most of the electron flux to the wall is created by the secondary electron beams. The expression for the total emission coefficient is[13,22]

$$\gamma = \frac{\Gamma_2}{\Gamma_p + \Gamma_b} = \frac{\gamma_p}{1 + \alpha(\gamma_p - \gamma_b)}. \tag{2}$$

The exact values of fluxes and emission coefficients in simulations satisfy these analytical relations. For the simulation presented in this section the total emission coefficient is $\gamma = 0.97$. Note that $\gamma < \gamma_{cr} = 0.983$ although the average energy of plasma electrons $\langle w \rangle = 66$ eV considerably exceeds the critical electron temperature $T_{cr} = 18.26$ eV obtained for the Maxwellian EVDF. The partial emission coefficient due to the plasma bulk electrons exceeds unity $\gamma_p > 1$. The primary electron flux due to the emitted electrons Γ_b about 6.8 times exceeds the primary electron flux of the bulk plasma electrons Γ_p.

The problem of the sheath formation in a bounded plasma slab in presence of the counterpropagating secondary electron beams has been considered in the fluid framework in Ref. 26. The effect of SEE produced by the beams of secondary electrons was not considered; thus the conclusions made in Ref. 26 relate to the case of weak accelerating fields. The results of Ref. 26 may be obtained as a particular case of more general equation (2).

The considered model reveals several features of plasma-wall interaction in Hall thrusters, which are missed by fluid theories as well as by kinetic simulations of near-wall regions carried out with the assumption that the bulk plasma has a Maxwellian EVDF. It is found that the thruster plasma is anisotropic, the secondary electrons almost freely propagate between the walls and produce secondary emission themselves. The criterion of the space-charge-limited secondary electron emission is modified: the average energy of electrons confined by the plasma potential may be large, while SEE remains in the non-SCL regime. There are several practical implications of these studies: (i) the strong SEE effect on power losses and near-wall conductivity in the thruster discharge is expected to occur only when the axial electric field provides the emitted electrons with sufficient additional energy; (ii) the SEE effect depends on the channel width because the energy of secondary electron beams at the moment of their impact with the walls depends on the time of electron transit between the walls. These predictions appear to be in an agreement with experimental studies.

[1]G. D. Hobbs and J. A. Wesson, Plasma Phys. **9**, 85 (1967).
[2]A. Smirnov, Y. Raitses, and N. J. Fisch, J. Appl. Phys. **94**, 852 (2003).
[3]E. Y. Choueiri, Phys. Plasmas **8**, 5025 (2001).
[4]M. Keidar, I. D. Boyd, and I. I. Beilis, Phys. Plasmas **8**, 5315 (2001).
[5]E. Ahedo, J. M. Gallardo, and M. Martinez-Sanchez, Phys. Plasmas **10**, 3397 (2003).
[6]S. Barral, K. Makowski, Z. Peradzynski, N. Gascon, and M. Dudeck, Phys. Plasmas **10**, 3397 (2003).
[7]Y. Raitses, D. Staack, A. Smirnov, and N. J. Fisch, Phys. Plasmas **12**, 073507 (2005).
[8]D. Staack, Y. Raitses, and N. J. Fisch, Appl. Phys. Lett. **84**, 3028 (2004).
[9]N. B. Meezan and M. A. Cappelli, Phys. Rev. E **66**, 036401 (2002).
[10]O. Batishchev and M. Martinez-Sanchez, *Proceedings of the 28th International Electric Propulsion Conference, Toulouse, France, March 2003* (Electric Rocket Propulsion Society, Cleveland, OH, 2003), IEPC Paper No. 2003-188.
[11]I. Kaganovich, M. Misina, S. V. Berezhnoi, and R. Gijbels, Phys. Rev. E **61**, 1875 (2000).
[12]D. Sydorenko and A. Smolyakov, Bull. Am. Phys. Soc. **49**, 261 (2004).
[13]D. Sydorenko, A. Smolyakov, I. Kaganovich, and Y. Raitses, *Proceedings of the 29th International Electric Propulsion Conference, Princeton, NJ, October–November 2005* (Electric Rocket Propulsion Society, Cleveland, OH, 2005), IEPC Paper No. 2005-078.
[14]A. B. Langdon, B. I. Cohen, and A. Friedman, J. Comput. Phys. **51**, 107 (1983).
[15]M. R. Gibbons and D. W. Hewett, J. Comput. Phys. **120**, 231 (1995).
[16]V. Vahedi and M. Surendra, Comput. Phys. Commun. **87**, 179 (1995).
[17]J. P. Boeuf and L. Garrigues, J. Appl. Phys. **84**, 3541 (1998).
[18]A. Smirnov, Y. Raitses, and N. Fisch, Phys. Plasmas **11**, 4922 (2004).
[19]V. P. Gopinath, J. P. Verboncoeur, and C. K. Birdsall, Phys. Plasmas **5**, 1535 (1998).
[20]A. Dunaevsky, Y. Raitses, and N. J. Fisch, Phys. Plasmas **10**, 2574 (2003).
[21]Y. Raitses, D. Staack, M. Keidar, and N. J. Fisch, Phys. Plasmas **12**, 057104 (2005).
[22]I. Kaganovich, *Proceedings of the 29th International Electric Propulsion Conference, Princeton, NJ, October–November 2005* (Electric Rocket Propulsion Society, Cleveland, OH, 2005), IEPC Paper No. 2005-096.
[23]L. A. Schwager, Phys. Fluids B **5**, 631 (1993).
[24]F. Taccogna, S. Longo, and M. Capitelli, Phys. Plasmas **12**, 093506 (2005).
[25]A. I. Morozov and V. V. Savel'ev, Plasma Phys. Rep. **27**, 570 (2001).
[26]E. Ahedo and F. I. Parra, Phys. Plasmas **12**, 073503 (2005).